



Peroxymonosulfate-enhanced visible light photocatalytic degradation of bisphenol A by perylene imide-modified g-C₃N₄



Juanjuan Zhang^{a,b}, Xu Zhao^{a,b,*}, Yanbin Wang^{a,c}, Yan Gong^a, Di Cao^{a,b}, Meng Qiao^a

^a Key Laboratory of Drinking Water Science and Technology, Research Center for Eco-Environmental Sciences, Chinese Academy of Sciences, Beijing 100085, PR China

^b University of Chinese Academy of Sciences, Beijing 100049, PR China

^c Key Laboratory for Yellow River and Huai River Water Environment and Pollution Control, Ministry of Education, School of Environment, Henan Normal University, Xinxiang, Henan 453007, PR China

ARTICLE INFO

Keywords:

g-C₃N₄
Photocatalysis
Peroxymonosulfate
Bisphenol A

ABSTRACT

In this study, a metal-free photocatalyst (PI-g-C₃N₄) was synthesized through an amidation reaction between perylene tetracarboxylic dianhydride (PTCDA) and graphitic carbon nitride (g-C₃N₄). In order to enhance the photocatalytic degradation efficiency of bisphenol A (BPA) by 5 wt% PI-g-C₃N₄, peroxyomonosulfate (PMS) was introduced into this system. When 5 mM PMS was added, 96% of BPA with an initial concentration of 10 mg/L was degraded within 60 min; the pseudo-first-order degradation kinetics constant of BPA was increased from 0.0057 to 0.0501 min⁻¹. Based on the photoelectrochemical analysis, it was proposed that PI-g-C₃N₄ achieved a more effective separation of photogenerated electron–hole pairs and displayed higher conductivity than PTCDA and g-C₃N₄ individually, thus promoting the PMS activation into active radicals by the photogenerated electrons. The BPA degradation was favored at high PMS concentrations under alkaline conditions. The slight inhibition effect of co-existing anions on the degradation of BPA followed the order: H₂PO₄⁻ > NO₃⁻ ≈ HCO₃⁻; Cl⁻ had a remarkable positive effect on the degradation of BPA. The radical quenching tests and electron spin resonance results indicated that O₂^{•-}, ¹O₂, and h⁺ were the major species for the degradation of BPA. Combined with intermediates analysis, the degradation mechanism and pathway of BPA was proposed. The high stability of the 5 wt% PI-g-C₃N₄ was finally demonstrated.

1. Introduction

Peroxymonosulfate (PMS)-based advanced oxidation processes (AOPs) have attracted an increasing research attention for the degradation of recalcitrant organic pollutants [1,2]. PMS can be activated to generate active radicals (such as SO₄²⁻, ·OH, and O₂^{•-}) by ultrasound, ultraviolet (UV) radiation, heat, metal ions, or metallic oxidant and nonmetal catalysts [3–9]. Of which, the catalytic activation by nonmetal catalysts is considered a sustainable and simple method without requiring extrinsic chemicals or external energy. Sun et al. [10] exhibited that rGO can effectively activate PMS to generate active radicals for degradation of organic contaminants. Zhang et al. [11] reported that PMS can be activated by granular activated carbon (GAC) to degrade Acid Orange 7 in aqueous solution.

Graphitic carbon nitride (g-C₃N₄), a polymeric semiconductor catalyst, is particularly attractive owing to its well-known metal-free nature, high stability, and easy preparation via cheap materials [12,13]. In previous reports, g-C₃N₄ was found to activate PMS for the

degradation of organic contaminants under visible light irradiation [14,15]. However, the main drawback of g-C₃N₄ is its low photocatalytic efficiency, mainly owing to the fast recombination of photogenerated electrons (e⁻) and holes (h⁺) [16,17]. A variety of attempts have been carried out to enhance the activation of PMS using g-C₃N₄, such as doping with elements [18,19], or by self-assembly [20]. Nevertheless, new approaches for g-C₃N₄ modification remain a research hotspot to further enhance its performance for PMS activation.

Perylene tetracarboxylic diimide (PTCDI) stands out among the available organic semiconductors owing to its wide visible light absorption, durable photostability, and good charge transportation properties [21]. It has a broad range of potential applications in the fields of biology, molecular chemistry, organic field effect transistors, material science, pharmacy, industrial coloring, medicine, etc. [22,23]. PTCDI can be synthesized via an amidation reaction between perylene tetracarboxylic dianhydride (PTCDA) and amine (–NH₂). As the edges of g-C₃N₄ have –NH₂ groups, it was reported that such amine groups could be reacted with PTCDA forming an all-solid-state Z-scheme

* Corresponding author at: Key Laboratory of Drinking Water Science and Technology, Research Center for Eco-Environmental Sciences, Chinese Academy of Sciences, Beijing 100085, PR China.

E-mail address: zhaoxu@rcees.ac.cn (X. Zhao).

heterojunction (PI-g-C₃N₄) to promote the photocatalytic performance for NO removal under visible light [24]. The introduction of PTCDA can provide stronger oxidizing power to holes and higher reducing power to electrons, resulting in a higher separation efficiency of the photo-generated electron–hole pairs. Thus, it is reasonable to assume that the combination of PTCDA and g-C₃N₄ will be an efficient approach to promote the PMS activation ability of g-C₃N₄, which is beneficial for the generation of active radicals. However, to the best of our knowledge, no research has been conducted on the utilization of PI-g-C₃N₄ to activate PMS for organic pollutant degradation.

In this study, we have constructed a metal-free visible light photocatalyst (PI-g-C₃N₄) with efficient activation of PMS for bisphenol A (BPA) degradation. The as-prepared PI-g-C₃N₄ catalyst was characterized, and its photocatalytic performance for PMS activation was evaluated. The influencing factors on the degradation of BPA were investigated, such as the PMS concentration, initial pH, and presence of co-existing anions. A possible mechanism was proposed based on radical quenching tests and electron spin resonance data. Moreover, after identification of the degradation intermediates, possible degradation pathways for BPA in the PI-g-C₃N₄/PMS/Vis system were proposed. As a green oxidation process, the activation of PMS with this metal-free PI-g-C₃N₄ photocatalyst is a valuable, promising, and feasible method for organic wastewater treatment.

2. Experimental

2.1. Chemicals

PTCDA was purchased from Alfa Aesar. PMS (2KHSO₅·KHSO₄·K₂SO₄) was purchased from Aladdin Chemistry Co. Ltd., China. 5,5-Dimethyl-1-pyrroline-N-oxide (DMPO) and 5-*tert*-butyloxycarbonyl-5-methyl-1-pyrroline-N-oxide (BMPO) were purchased from DOJINDO. 2,2,6,6-Tetramethyl-4-piperidone (4-oxo-TEMP) was purchased from Sigma-Aldrich. Imidazole (C₃H₄N₂), melamine (C₃N₃(NH₂)₃), *tert*-butyl alcohol (C₄H₁₀O, TBA), methanol (CH₃OH, MeOH), ethanol (CH₃CH₂OH, EtOH), disodium ethylenediaminetetraacetate (EDTA-2Na), *p*-benzoquinone (*p*-BQ), L-histidine (C₆H₉N₃O₂), sodium chloride (NaCl), potassium carbonate (K₂CO₃), sodium dihydrogen phosphate (NaH₂PO₄), sodium sulfate (Na₂SO₄), sodium bicarbonate (NaHCO₃), and sodium nitrate (NaNO₃) were obtained from Sinopharm Chemical Reagent Co., Ltd., China. Bisphenol A (C₁₅H₁₆O₂, BPA), phenol (C₆H₅OH, PhOH), 2,4-dichlorophenol (C₆H₄Cl₂O, 2,4-DCP), *p*-nitrophenol (C₆H₅NO₃, *p*-NP), *p*-hydroxybenzoic acid (C₇H₆O₃, *p*-HBA), and benzoic acid (C₆H₅COOH, BA) were obtained from TCI, Japan. All chemicals were used as obtained without any further purification. Milli-Q water ($\rho = 18.2 \text{ M}\Omega \text{ cm}$) produced on a Milli-Q purification system (Millipore, Billerica, MA) was used in all experiments. The pH of the solutions was adjusted with either H₂SO₄ (0.1 M) or NaOH (0.1 M) in a PHS-3E pH meter.

2.2. Preparation and characterization of photocatalysts

Firstly, g-C₃N₄ was prepared by direct calcination of melamine [25]. A certain amount of melamine was placed in a covered ceramic crucible, then calcined at 520 °C with a heating rate of 20 °C/min and finally held at 520 °C for 4 h. The final yellow powder of g-C₃N₄ was obtained after grinding. PI-g-C₃N₄ was synthesized according to a previous study with a slight modification [24]. A series of PI-g-C₃N₄ catalysts with diverse loading of PTCDA were prepared. And the as-prepared catalysts were defined as x wt% PI-g-C₃N₄ (x represents the weight percentage of PTCDA, x = 1, 3, 5, 7, and 10). PI-g-C₃N₄ was synthesized through an amidation reaction between PTCDA and g-C₃N₄. Briefly, an appropriate amount of PTCDA, 2.84 g of g-C₃N₄, and 10 g of imidazole were placed in a quartz crucible, followed by heating at 140 °C for 5 h under nitrogen atmosphere. Subsequently, the mixture was suspended in 200 mL ethanol at ambient temperature (20–25 °C)

with stirring. Then, the solution was transferred to 600 mL of HCl (2 M). After 12 h, the mixture solution was centrifuged and washed with methanol and Milli-Q water. The resulting powder was transferred to 200 mL of a K₂CO₃ solution (10%), which was placed in an oil bath at 100 °C for 1 h under reflux. After the reaction solution cooled down to 50 °C, it was centrifuged and washed for three times with 600 mL of a K₂CO₃ solution (10%), followed by 200 mL of HCl (2 M). Next, the powder was finally washed thoroughly with methanol and Milli-Q water until the pH of the rinsed water was neutral. Ultimately, the obtained powder (x wt% PI-g-C₃N₄) was dried under vacuum at 80 °C for 12 h. We performed all experiments using 5 wt% PI-g-C₃N₄ unless the effect of different PTCDA loading was studied.

X-ray diffraction (XRD) analysis was conducted on an X-ray diffractometer (X'pert Pro MPD) using Cu K α radiation (40 kV, 40 mA, $\lambda = 1.540\text{562}\text{\AA}$). Field emission-scanning electron microscopy (FE-SEM) images were acquired on a SU8010 instrument (HITACHI, Japan). Transmission electron microscopy (TEM) was performed on a H7500 instrument (HITACHI, Japan). X-ray photoelectron microscopy (XPS) images were recorded on a PHI Quanta XRM instrument (ULVAC-PHI, Japan) under Al Ka X-rays. The binding energy was calibrated using a carbon impurity (C 1s = 284.8 eV). Fourier transform infrared (FT-IR) spectra were obtained on a Bruker Vector 22 spectrometer. N₂ adsorption-desorption isotherms of the as-prepared photocatalysts were obtained using ASAP2020 HD88 instrument (Micromeritics, USA) at $-196\text{ }^{\circ}\text{C}$. The specific surface area was estimated by Brunauer–Emmett–Teller (BET) method. Diffuse reflectance UV-vis absorption spectra (UV-vis DRS) of the as-prepared catalysts were recorded on a UV-vis spectrometer (Hitachi 3010, Japan) using BaSO₄ as the reflectance standard reference; the data were then converted from reflection to absorbance by the Kubelka–Munk method. Electron spin resonance (ESR) measurements were carried out at ambient temperature on a Bruker EMX (A300-10/12, Germany) with a microwave bridge (modulation frequency, 100 kHz; microwave frequency, 9.85 GHz; modulation amplitude, 1 G; microwave power, 22.8 mW).

2.3. Photocatalytic experiments

The experiments for the photocatalytic degradation of BPA by the as-prepared catalysts were carried out in a rectangular quartz reactor (120 mL, 50 × 50 × 50 mm³). A BPA solution (100 mL, 10 mg/L) containing 1 g/L of the catalysts was transferred into the reactor and stirred for 10 min to reach the adsorption–desorption equilibrium between the catalysts and BPA. Then, a certain amount of PMS was added to the suspension. A 300 W Xe lamp (PLS-SXE300; Beijing Perfect Light Co., Ltd, Beijing, China) with a 400 nm cutoff was selected as the visible light source. During the photocatalytic reaction, 500 μL aliquots of the suspension were taken from the photocatalytic reactor at regular times, immediately mixed with 500 μL methanol, and then filtered through a Millipore filter (pore size of 0.22 μm) for high performance liquid chromatography (HPLC) analysis.

2.4. Photoelectrochemical experiments

Photoelectrochemical experiments were conducted in a conventional three-electrode system. Specifically, a saturated calomel electrode (SCE), the as-prepared photoelectrodes, and a Pt wire served as the reference, working, and counter electrodes, respectively. The experiments were performed on an electrochemical workstation (CHI660E, Chenhua Instrument Co. Ltd., Shanghai, China). The photoelectrodes were prepared following a previously reported method [19]. Typically, 10 mg of the photocatalyst was dispersed in a mixture of a Nafion solution (200 μL , 5%) and ethanol (800 μL), which was ultrasonicated for 180 min to form a uniform suspension. Indium-tin oxide (ITO; 10 × 30 × 1.1 mm; 15 Ω) glass was used as electrode substrate material for fabricating photoelectrodes [26]. 100 μL of suspension were dip-coated on the ITO glass and dried overnight at

ambient temperature. Finally, the $\text{g-C}_3\text{N}_4$ /ITO, PTCDA/ITO and PI- C_3N_4 /ITO composite electrodes were obtained. The working electrode was irradiated from the opposite side of the as-prepared film under a 300 W Xe lamp with a 400 nm cutoff. In the experiments, the photo-electrode (described above) was placed in a 100 mM Na_2SO_4 aqueous solution. In Mott–Schottky experiments, the perturbation signal was measured at a frequency of 100 Hz. Electrochemical impedance spectroscopy (EIS) analyses of $\text{g-C}_3\text{N}_4$, PTCDA, and PI- $\text{g-C}_3\text{N}_4$ were carried out by sweeping the frequency from 100,000 Hz to 0.01 Hz with AC amplitude at open circuit potential.

2.5. Analytical methods

The concentration of BPA was analyzed on an HPLC (Shimadzu LC-20AT, Tokyo, Japan) equipped with a UV detector ($\lambda = 276$ nm) and an EC-C18 column (250 mm \times 4.6 mm \times 5 μm , GL Science Inc., Tokyo, Japan). The mobile phase was a mixture of water and methanol ($\text{v/v} = 30/70$) at a flow rate of 1 mL/min. The injection volume was 20 μL . The analysis of the intermediate products was performed by ultra-performance liquid chromatography-quadrupole time-of-flight mass spectrometry (UPLC-Q-TOF-MS, ACQUITY UPLC, Quattro Premier XE, Waters, USA) with a C18 column (50 mm \times 2.1 mm \times 1.7 μm). The mobile phase involved Milli-Q water (A) and methanol (B) solvents with a flow rate of 0.3 mL/min. The elution gradient was as follows: 99% A and 1% B for 15 min, 80% A and 20% B for 10 min, 50% A and 50% B for 10 min, and 99% A and 1% B for 4 min. MS and MS/MS analyses were carried out in negative electrospray ionization (ESI⁻) mode in the m/z range of 50–800. The total organic carbon (TOC) of BPA was determined with a vario TOC analyzer (Elementar, Germany). For ESR measurements, a 10 μL aliquot was taken from the reaction solution and then immediately mixed with 10 μL of 160 mM DMPO, 25 mM BMPO, and 5 mM TEMP.

3. Results and discussion

3.1. Photocatalyst characterization

Firstly, the structure of the as-prepared photocatalysts was characterized. As shown in Fig. 1, the color of $\text{g-C}_3\text{N}_4$ is light yellow while PTCDA is bright red. After the reaction, the final color of 5 wt% PI- $\text{g-C}_3\text{N}_4$ is pink, implying the formation of a new substance. However, the XRD spectrum of 5 wt% PI- $\text{g-C}_3\text{N}_4$ exhibits only the two characteristic peaks of $\text{g-C}_3\text{N}_4$ [27]. No diffraction peaks for the PTCDA phase is observed. This phenomenon might be due to the low density of $-\text{NH}_2$ groups distributed along the edges of $\text{g-C}_3\text{N}_4$, from which the PTCDA molecules are sparsely distributed on the surface of $\text{g-C}_3\text{N}_4$. The overall

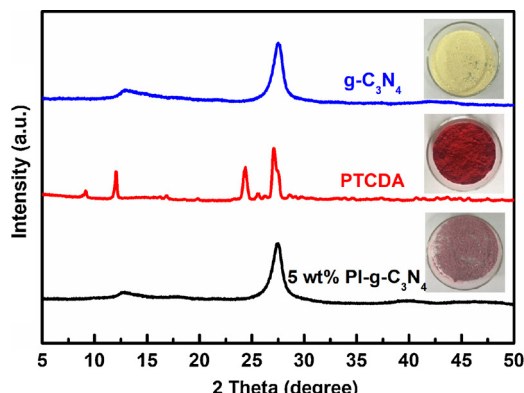


Fig. 1. XRD patterns of $\text{g-C}_3\text{N}_4$, PTCDA, and 5 wt% PI- $\text{g-C}_3\text{N}_4$ (insets: photographs of the $\text{g-C}_3\text{N}_4$ (yellow), PTCDA (red), and 5 wt% PI- $\text{g-C}_3\text{N}_4$ (pink) solids (For interpretation of the references to color in this figure legend, the reader is referred to the web version of this article).

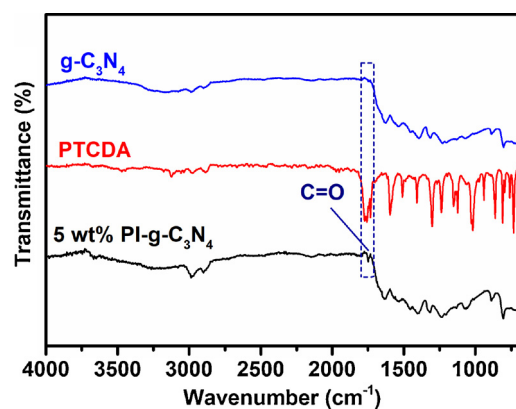


Fig. 2. FT-IR spectra of $\text{g-C}_3\text{N}_4$, PTCDA, and 5 wt% PI- $\text{g-C}_3\text{N}_4$.

platelet-like morphology of $\text{g-C}_3\text{N}_4$ is maintained after the surface modification with PTCDA, as shown by the SEM and TEM images (Fig. S1).

To further confirm that PTCDA was successfully attached to the surface of $\text{g-C}_3\text{N}_4$, the FT-IR spectra of $\text{g-C}_3\text{N}_4$, PTCDA and 5 wt% PI- $\text{g-C}_3\text{N}_4$ were recorded to analyze their functional groups (Fig. 2). For $\text{g-C}_3\text{N}_4$ and 5 wt% PI- $\text{g-C}_3\text{N}_4$, the broad bands at 1200–1600 cm^{-1} correspond to the stretching vibration modes of C–N heterocycles, containing either bridging C–N–C or trigonal N–C₃ units [28–30]. In addition, the band located at 809 cm^{-1} is the typical breathing mode of the s-triazine ring [31]. In the case of PTCDA, the peak around 1751 cm^{-1} is the characteristic absorption bands of C=O bond [32]. For 5 wt% PI- $\text{g-C}_3\text{N}_4$, the band at 1749 cm^{-1} corresponding to the bending vibration of C=O bond is clearly observed, confirming the presence of PTCDA in 5 wt% PI- $\text{g-C}_3\text{N}_4$.

The XPS technique was employed to analyze the composition and chemical states of $\text{g-C}_3\text{N}_4$, PTCDA and 5 wt% PI- $\text{g-C}_3\text{N}_4$. Three elements C, N, and O are detected in the survey spectra of $\text{g-C}_3\text{N}_4$ and 5 wt% PI- $\text{g-C}_3\text{N}_4$, while only two elements C and O are detected in PTCDA (Fig. 3a). As shown in Fig. 3b, for $\text{g-C}_3\text{N}_4$ and 5 wt% PI- $\text{g-C}_3\text{N}_4$, the C 1s peaks at 286.3 and 284.8 eV correspond to sp^2 C–NH₂ species and C–C bonds, respectively [33]. In addition, the C 1s peaks at 288.1–288.5 eV are ascribed to sp^2 -hybridized carbon atoms (N–C=N) [34]. In the case of PTCDA, the C 1s peaks at 288.6 and 284.8 eV correspond to the dianhydride carboxylic groups of the molecule and C–C bonds, respectively [35,36]. It can be observed that the decrease of the intensity of the N–C=N peak for 5 wt% PI- $\text{g-C}_3\text{N}_4$ compared to that for the C–C peak. This phenomenon may be explained by a reduction of the amount of N–C=N bonds resulting from the amidation reaction between $\text{g-C}_3\text{N}_4$ and PTCDA [37]. As shown in Fig. 3c, both $\text{g-C}_3\text{N}_4$ and PI- $\text{g-C}_3\text{N}_4$ samples exhibit an O 1s peak at 532.6 eV, which is assigned to the surface adsorbed H_2O molecules or hydroxyl groups [38]. PTCDA exhibits two O 1s peaks at 533.3 and 531.6 eV correspond to C–O–C bonds and C=O bonds, respectively [35]. However, compared with $\text{g-C}_3\text{N}_4$, the spectrum of 5 wt% PI- $\text{g-C}_3\text{N}_4$ shows a new peak at 531.0 eV, which is ascribed to C–O or carbonyl groups, indicating the formation of imide groups in PI- $\text{g-C}_3\text{N}_4$ [24]. The N 1s spectrum of the $\text{g-C}_3\text{N}_4$, PTCDA and 5 wt% PI- $\text{g-C}_3\text{N}_4$ samples are shown in Fig. 3d. No obvious N 1s peak is observed in PTCDA. The N 1s spectrum of $\text{g-C}_3\text{N}_4$ is deconvoluted into two peaks at 398.7 and 401.0 eV. The peak at 398.7 eV is attributed to the sp^2 -hybridized N atoms (C–N–C) in the triazine ring, while the peak at 401.0 eV is ascribed to the bridging N atoms (C–N₃) of the melem unit [39,40]. Besides these two peaks, an additional peak at 400.2 eV appears in the N 1s spectrum of 5 wt% PI- $\text{g-C}_3\text{N}_4$, which can be assigned to the imide N atoms (O=C–N–C=O) [41]. These results indicate that the reaction between PTCDA and the amino groups is successful and that PTCDA is attached to the $\text{g-C}_3\text{N}_4$ surface.

As shown in Fig. 4a, 5 wt% PI- $\text{g-C}_3\text{N}_4$ absorbs more visible light than

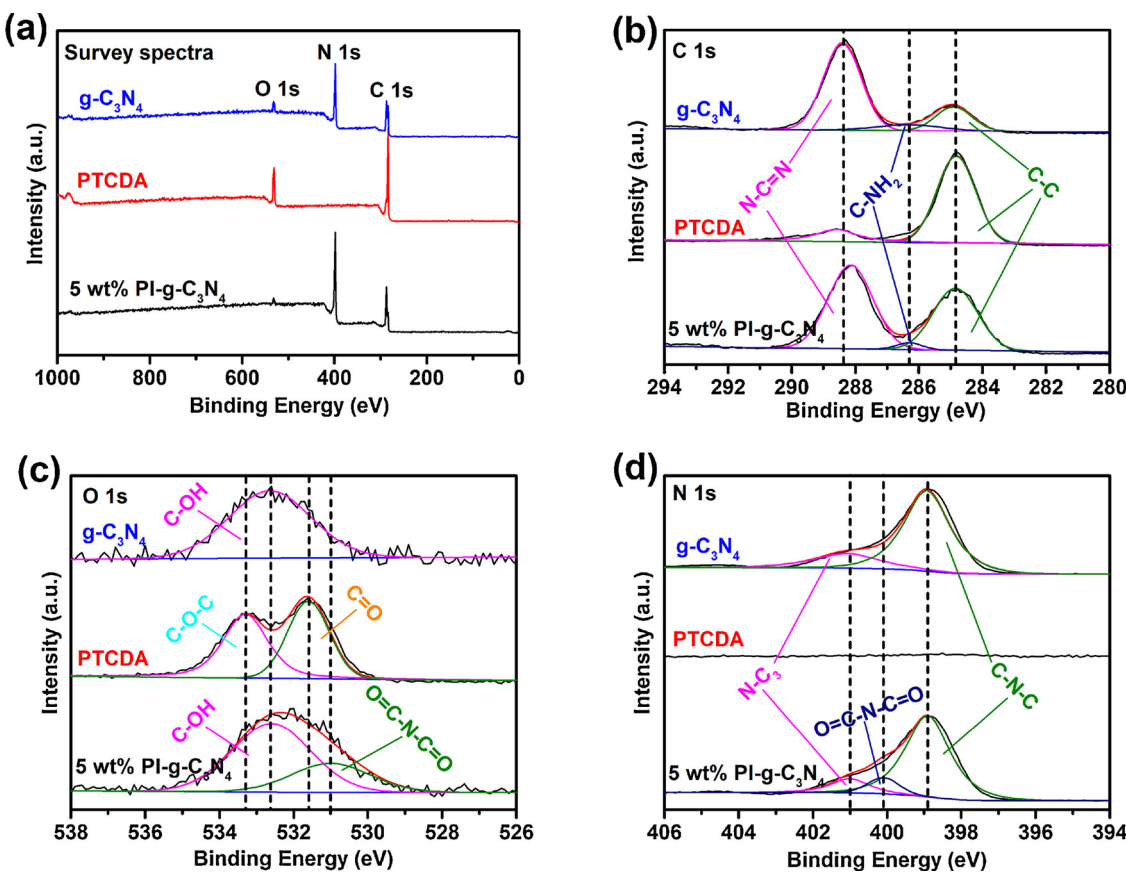


Fig. 3. XPS spectra of $\text{g-C}_3\text{N}_4$, PTCDA, and 5 wt% PI- $\text{g-C}_3\text{N}_4$: (a) survey spectra, (b) C 1s, (c) O 1s, (d) N 1s.

$\text{g-C}_3\text{N}_4$ and PTCDA, in agreement with the color change from yellow ($\text{g-C}_3\text{N}_4$) to pink (5 wt% PI- $\text{g-C}_3\text{N}_4$). The Tauc plot reveals the band gap energy for 5 wt% PI- $\text{g-C}_3\text{N}_4$ of 1.75 eV, smaller than those of $\text{g-C}_3\text{N}_4$ (2.53 eV) and PTCDA (1.90 eV) (Fig. 4b). It can be concluded that 5 wt% PI- $\text{g-C}_3\text{N}_4$ exhibits enhanced performance for visible light absorption.

The BET specific surface area plays an important role on the photocatalyst. N_2 adsorption–desorption isotherms of $\text{g-C}_3\text{N}_4$, PTCDA and 5 wt% PI- $\text{g-C}_3\text{N}_4$ were obtained to analyze the BET surface areas of as-prepared photocatalysts (Fig. 5). The BET surface areas of $\text{g-C}_3\text{N}_4$, PTCDA and 5 wt% PI- $\text{g-C}_3\text{N}_4$ were calculated to be *ca.* 9.287, 15.422 and $21.640 \text{ m}^2/\text{g}$, respectively. The introduction of PTCDA into the matrix of $\text{g-C}_3\text{N}_4$ shows a little influence on the BET surface area. This result indicates that the surface area may not be the main factor accounting for the different photocatalytic activities of the $\text{g-C}_3\text{N}_4$, PTCDA and 5 wt% PI- $\text{g-C}_3\text{N}_4$.

3.2. Photocatalytic activity

Firstly, the adsorption experiments and chemical activation of PMS were performed under dark condition. The $\text{g-C}_3\text{N}_4$, PTCDA, and 5 wt% PI- $\text{g-C}_3\text{N}_4$ has no obvious adsorption toward BPA (Fig. S2a). After addition of 5 mM PMS, BPA degradation is slightly improved, indicating the poor reactivity toward PMS activation (Fig. S2b). As shown in Fig. S3, the degradation of BPA by only PMS is negligible under dark condition, and 27% BPA is degraded under visible light irradiation, indicating that PMS can slightly promote the photocatalytic degradation of BPA. The photocatalytic activity of $\text{g-C}_3\text{N}_4$, PTCDA, and 5 wt% PI- $\text{g-C}_3\text{N}_4$ for BPA degradation was compared under visible light irradiation. As shown in Fig. 6a, within 60 min, only 6% and 5% BPA (initial concentration of 10 mg/L) is degraded by $\text{g-C}_3\text{N}_4$ and PTCDA, respectively. By contrast, 29% BPA is removed by 5 wt% PI- $\text{g-C}_3\text{N}_4$. It can be

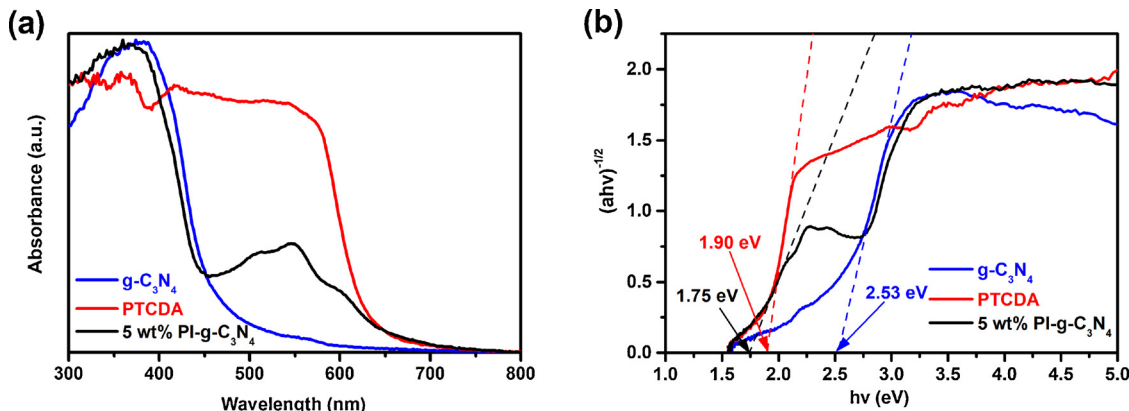


Fig. 4. (a) Diffuse reflectance UV-vis spectra and (b) Tauc plots for $\text{g-C}_3\text{N}_4$, PTCDA, and 5 wt% PI- $\text{g-C}_3\text{N}_4$.

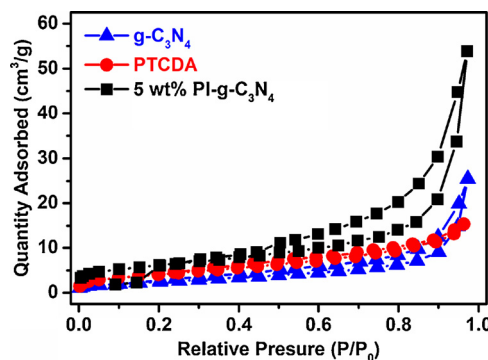


Fig. 5. N_2 adsorption-desorption isotherms of $\text{g-C}_3\text{N}_4$, PTCDA, and 5 wt% PI- $\text{g-C}_3\text{N}_4$.

seen that 5 wt% PI- $\text{g-C}_3\text{N}_4$ shows an enhanced photocatalytic performance, which may be due to a synergistic effect of PTCDA and $\text{g-C}_3\text{N}_4$. With the addition of 5 mM PMS, the degradation efficiency of BPA is increased up to 96%. As shown in Fig. 6b, the degradation of BPA follows pseudo-first-order kinetics. The kinetic constants are determined to be 0.0009 ($R^2 = 0.960$), 0.0012 ($R^2 = 0.971$), 0.0015 ($R^2 = 0.918$), 0.0057 ($R^2 = 0.986$), 0.0066 ($R^2 = 0.910$) and 0.0501 min^{-1} ($R^2 = 0.960$) for PTCDA, $\text{g-C}_3\text{N}_4$, $\text{g-C}_3\text{N}_4/\text{PMS}$, 5 wt% PI- $\text{g-C}_3\text{N}_4$, PTCDA/PMS, and 5 wt% PI- $\text{g-C}_3\text{N}_4/\text{PMS}$ systems under visible light irradiation, respectively. These results demonstrate that PMS can greatly enhance the photocatalytic degradation efficiency of BPA by 5 wt% PI- $\text{g-C}_3\text{N}_4$.

3.3. Influencing factors on the photocatalytic degradation

The effect of different PTCDA loading in the PI- $\text{g-C}_3\text{N}_4$ composites on the degradation of BPA was investigated in detail. As shown in Fig. 7a, the degradation efficiency of BPA are 92%, 90%, 96%, 90% and 87% with PTCDA weight percentages increasing from 1 wt% to 10 wt%, respectively. The 5 wt% PI- $\text{g-C}_3\text{N}_4$ photocatalyst exhibits the highest kinetic constants for the degradation of BPA. The degradation rate of BPA over 7 wt% PI- $\text{g-C}_3\text{N}_4$ and 10 wt% PI- $\text{g-C}_3\text{N}_4$ is lower than 5 wt% PI- $\text{g-C}_3\text{N}_4$, which may be explained by the much amount of PTCDA in PI- $\text{g-C}_3\text{N}_4$ could lead to the low migration and separation rate of the photogenerated charges [42]. Therefore, an appropriate loading amount of PTCDA in the PI- $\text{g-C}_3\text{N}_4$ is important.

As shown in Fig. 7b, the degradation of BPA increases gradually with the PMS dosage in the range from 0 to 10 mM. The kinetic constants subsequently increase from 0.0057 to 0.0611 min^{-1} . With the addition of 5 mM PMS, 96% BPA is degraded within 60 min. Nevertheless, when the PMS dosage is increased to 10 mM, only a slight

increase in BPA removal is observed. Wang et al. [43] found that high PMS dosages generated more active radicals for the degradation process. However, when 10 mM PMS was added, the number of photo-generated electrons might be not enough to activate the PMS in this system [19]. As shown in Fig. S4, the TOC removal efficiency increases from 5% to 54% with the PMS dosage from 0 to 10 mM. The removal ratio of TOC increases with the PMS dosage. It is concluded that BPA can be more efficiently degraded in the PI- $\text{g-C}_3\text{N}_4/\text{PMS}/\text{Vis}$ system with the increasing PMS dosage.

The effect of the initial pH on the degradation of BPA by the 5 wt% PI- $\text{g-C}_3\text{N}_4/\text{PMS}/\text{Vis}$ system was investigated. As shown in Fig. 7c, the BPA degradation efficiency is significantly enhanced as the initial solution pH increased from 3.0 to 11.0, and the kinetic constants for BPA degradation increases from 0.0309 to 0.0854 min^{-1} . However, the differences in the BPA degradation rates in the pH range from 3.0 to 9.0 are not obvious, possibly due to the acidification induced by PMS. When 5 mM PMS was present, a rapid decrease in the pH value was observed when the initial pH was 3.0 to 9.0, and the final pH dropped to 2.9, 3.6, 4.8, and 5.2 after the reaction, respectively. When the initial pH was 11.0, the final pH was 10.4. It has been reported that the pK_a value of PMS is 9.4 [44], which means that H_2SO_5 is the major form of PMS when the solution pH is below 9.4. Therefore, the activation of PMS is inhibited at initial pH values equal or over 9. The BPA degradation rate with an initial pH 11.0 was much faster than that at other values, possibly benefiting from a slower dropping rate of pH [45]. Therefore, it can be concluded that PMS is more likely to be activated for the generation of active radicals under alkaline conditions, thus enhancing the degradation efficiency of BPA [14].

Some anions, such as Cl^- , HCO_3^- , H_2PO_4^- , NO_3^- , and SO_4^{2-} may affect the degradation efficiency of organic pollutants. As shown in Fig. 7d, H_2PO_4^- , NO_3^- , and HCO_3^- exhibit a slightly inhibiting effect on the degradation of BPA, and the inhibition efficiency follows the order: $\text{H}_2\text{PO}_4^- > \text{NO}_3^- \approx \text{HCO}_3^-$. SO_4^{2-} does not display effect on the BPA degradation while Cl^- has a remarkable positive effect. It is known that H_2PO_4^- sometimes serves as a radical scavenger in AOPs [19]. As a consequence, the inhibition on the BPA degradation by H_2PO_4^- might be due to the generated reactive species. HCO_3^- also usually acts as an $\cdot\text{OH}$ scavenger in AOPs [3]. However, the effect of HCO_3^- on the degradation of BPA is slight, suggesting that $\cdot\text{OH}$ radicals are likely not the major reactive species for BPA degradation. The degradation rate of BPA is slightly inhibited in the presence of NO_3^- , which can be explained by its reaction with SO_4^{2-} and $\cdot\text{OH}$ [46]. It is worth noting the remarkable positive effect of Cl^- on the degradation of BPA. Therefore, the effect of Cl^- on the degradation of BPA was further investigated at different Cl^- concentrations (Fig. S5). Increases in the Cl^- concentration resulted in an obvious increase in the degradation rate of BPA. As we know, Cl^- can be oxidized by both PMS

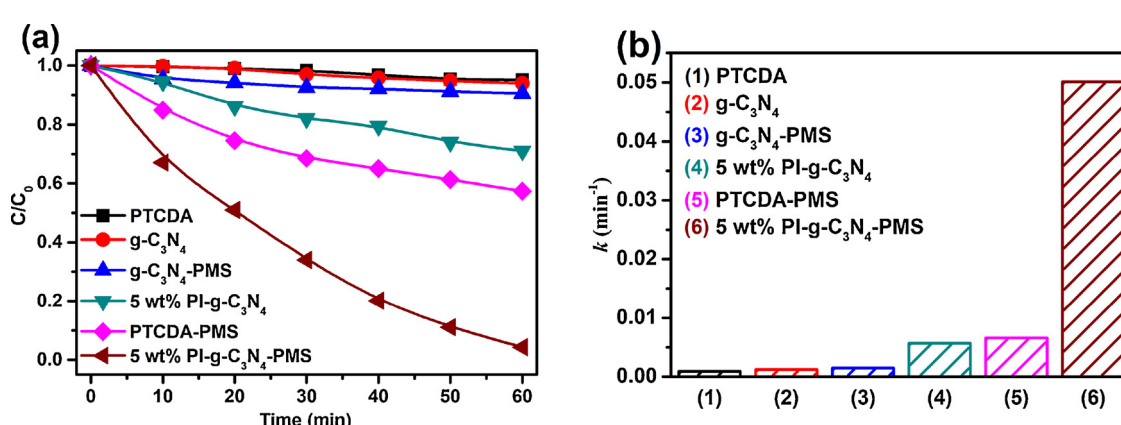


Fig. 6. (a) The degradation of BPA under visible light irradiation with different catalysts and (b) the corresponding kinetic constants. Conditions: $[\text{BPA}]_0 = 10 \text{ mg/L}$, $[\text{PMS}] = 5 \text{ mM}$, $[\text{Cat.}] = 1 \text{ g/L}$, $\lambda > 400 \text{ nm}$, ambient temperature, no buffer.

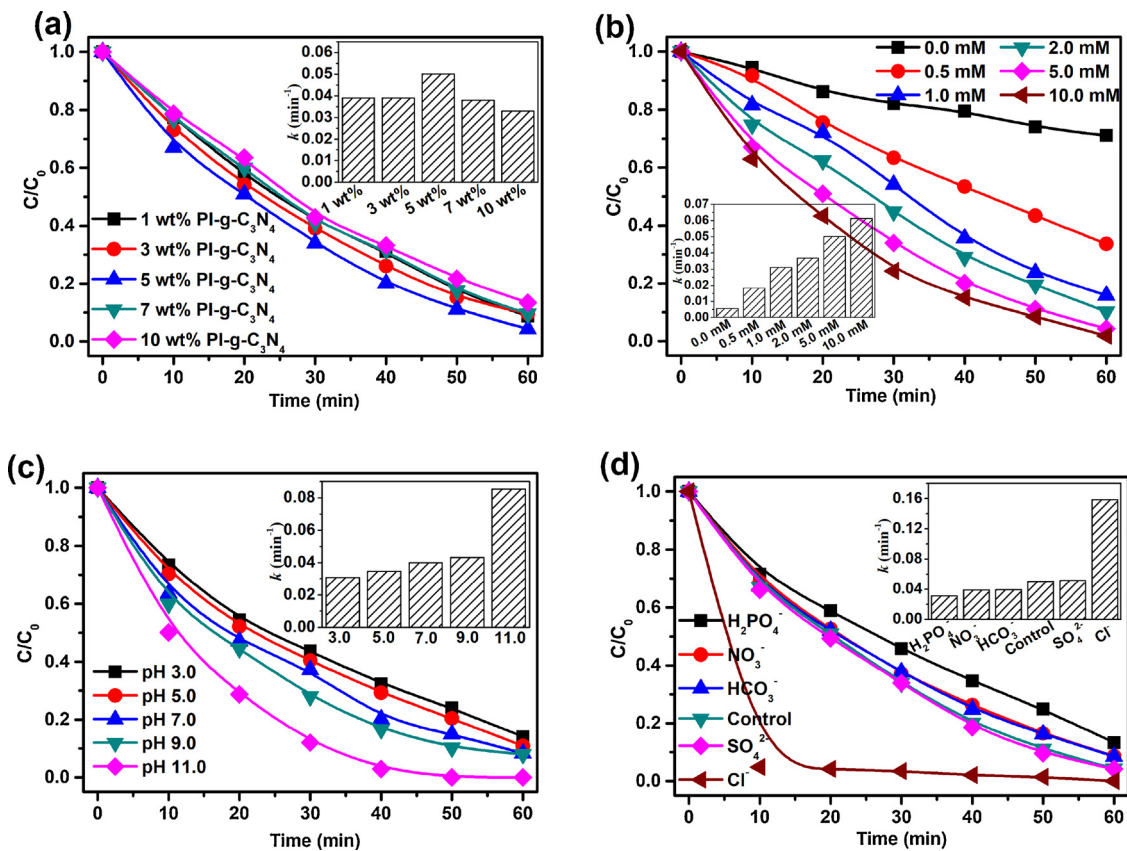


Fig. 7. Influencing factors on the BPA removal efficiency in the PI-g-C₃N₄/PMS/Vis system: (a) different PTCDA loading (inset: corresponding kinetic constants), (b) PMS concentration (inset: corresponding kinetic constants), (c) initial pH (inset: corresponding kinetic constants), and (d) influence of anions (5 mM) (inset: corresponding kinetic constants). Conditions: [BPA]₀ = 10 mg/L, [Cat.] = 1 g/L, $\lambda > 400$ nm, ambient temperature, no buffer.

and SO₄²⁻ to generate active chlorine species [47]. In the presence of Cl⁻ and PMS, active chlorine species (e.g., HOCl, Cl₂, and Cl[·]) may also be generated through nonradical pathways (Eqs. (1) and (2)) and SO₄²⁻-based pathways (Eqs. (3) and (4)). Therefore, active chlorine may contribute to the degradation of BPA in the PI-g-C₃N₄/PMS/Vis system.



The performance of the 5 wt% PI-g-C₃N₄/PMS system in the degradation of six typical recalcitrant organic compounds including BPA, BA, 2,4-DCP, PhOH, *p*-NP, and *p*-HBA was investigated to evaluate its potential for practical applications. As shown in Fig. 8, all the target compounds are efficiently degraded within 60 min. This result indicates that the 5 wt% PI-g-C₃N₄/PMS/Vis system offers a good versatility for organic wastewater treatment.

3.4. Photoelectrochemical properties

Based on the photoelectrochemical analysis, it was proposed that 5 wt% PI-g-C₃N₄ achieved a more effective separation of photogenerated electron-hole pairs and displayed higher conductivity than PTCDA and g-C₃N₄ individually, thus promoting the PMS activation into active radicals by the photogenerated electrons.

To further understand the contribution of PTCDA in the photocatalytic performance of 5 wt% PI-g-C₃N₄, photoelectrochemical measurements were performed. As shown in Fig. 9a, the transient

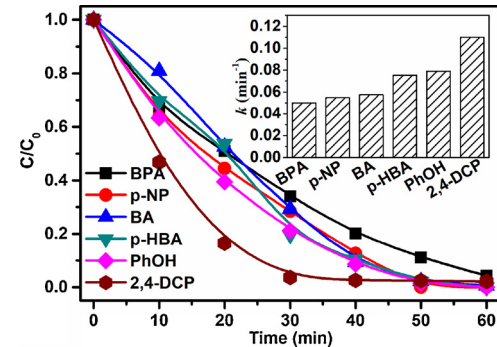


Fig. 8. The degradation of six organic pollutants by the 5 wt% PI-g-C₃N₄/PMS/Vis system (inset: kinetic constants). Conditions: [pollutant]₀ = 10 mg/L, [PMS] = 5 mM, [Cat.] = 1 g/L, $\lambda > 400$ nm, ambient temperature, no buffer.

photocurrent response of 5 wt% PI-g-C₃N₄, PTCDA, and g-C₃N₄ is monitored for several on-off cycles at 0 V (vs. SCE). The photocurrent intensity of PI-g-C₃N₄ exhibits an obvious enhancement compared to that of PTCDA and g-C₃N₄, indicating the superior separation efficiency of photogenerated charge carriers in 5 wt% PI-g-C₃N₄ [48].

With respect to the EIS results (Fig. 9b), 5 wt% PI-g-C₃N₄ exhibits a lower charge transfer resistance with a smaller semicircle radius than those for g-C₃N₄ and PTCDA, indicating that 5 wt% PI-g-C₃N₄ experiences a more effective separation process of photogenerated electron-hole pairs [26,49,50].

The oxidation and reduction ability of photogenerated holes and electrons is dependent on the valence band potential (V_{VB}) and conduction band (V_{CB}) potential, respectively [51]. The flat band potential (V_{FB}) is approximately equal to the V_{CB} or the V_{VB} in n-type or p-type

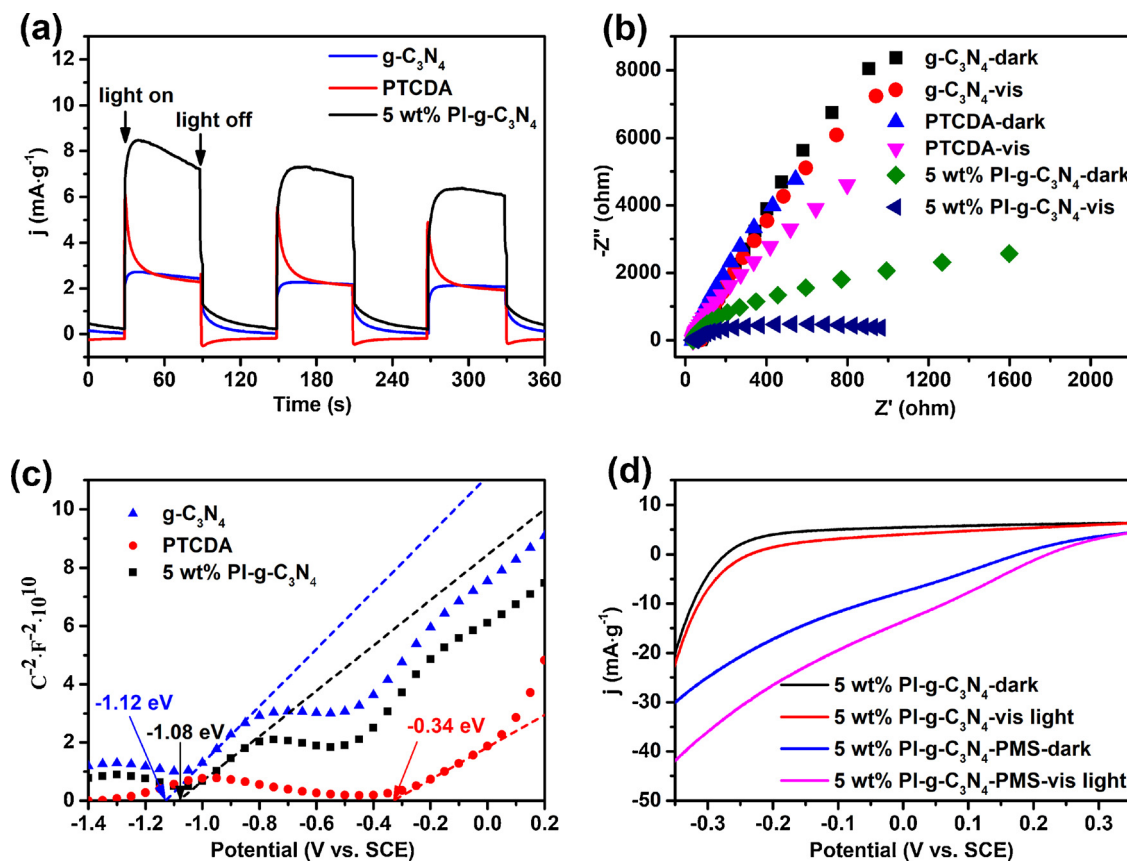


Fig. 9. (a) Transient photocurrent response of different photocatalysts at 0 V bias (vs. SCE), (b) EIS Nyquist in the presence or absence of visible light irradiation, (c) M-S plots measured at a frequency of 100 Hz in the dark, and (d) linear scanning voltammetry curves in the presence or absence of 5.0 mM PMS. Conditions: $[\text{Na}_2\text{SO}_4] = 100 \text{ mM}$, $\lambda > 400 \text{ nm}$, ambient temperature, no buffer.

semiconductors, respectively [52,53]. The Mott–Schottky (M–S) plots for g-C₃N₄, PTCDA and 5 wt% PI-g-C₃N₄ were obtained to analyze the nature of the semiconductor and the V_{FB} value. As shown in Fig. 9c, all of g-C₃N₄, PTCDA and 5 wt% PI-g-C₃N₄ display n-type semiconductor characteristics. The calculated V_{FB} values for g-C₃N₄, PTCDA and 5 wt% PI-g-C₃N₄ are -1.12 , -0.34 and -1.08 V (vs. SCE), corresponding to -0.88 , -0.10 and -0.84 V (vs. NHE), respectively. These results indicate that the V_{CB} of g-C₃N₄, PTCDA and 5 wt% PI-g-C₃N₄ are obviously more negative than that of $\text{SO}_4^{2-}/\text{SO}_4^{2-}$ ($2.5\text{--}3.1 \text{ V}$ vs. NHE) [54], meeting the thermodynamic requirements for PMS activation to generate SO_4^{2-} [55].

To verify the role of PMS in the photocatalytic process, linear scanning voltammetry (LSV) curves were measured in the absence or presence of PMS (Fig. 9d). The current of PI-g-C₃N₄ under visible light irradiation is higher than in the dark. In the presence of PMS, the current is significantly enhanced both under visible light irradiation and dark conditions. Moreover, the 5 wt% PI-g-C₃N₄/PMS/Vis system shows the highest photocurrent response. The reason of the increased current upon PMS addition could be explained by PMS acting as an electron acceptor, thus enhancing the transmission efficiency of photogenerated electrons.

3.5. Involved active species and proposed degradation mechanism

To explore the photocatalytic mechanism in the 5 wt% PI-g-C₃N₄/PMS/Vis system, the involved reactive oxygen species (ROS) were firstly analyzed by quenching experiments using different scavengers, such as TBA for $\cdot\text{OH}$ [3], MeOH for both $\cdot\text{OH}$ and SO_4^{2-} [5], p-BQ for $\text{O}_2\cdot^-$ [56], EDTA-2Na for h^+ [57,58], and L-histidine for $^1\text{O}_2$ [45]. As shown in Fig. 10a and b, the inhibition performance for the degradation of BPA follows the order: p-BQ > EDTA-2Na > L-histidine >

MeOH > TBA, and the kinetic constants for BPA degradation increases from 0.0013 to 0.0332 min^{-1} , indicating that $\text{O}_2\cdot^-$, h^+ , $^1\text{O}_2$, SO_4^{2-} , and $\cdot\text{OH}$ are responsible for the degradation of BPA. Among them, in the presence of p-BQ, EDTA-2Na, or L-histidine, the degradation of BPA is clearly inhibited. These results indicate that the active species including $\text{O}_2\cdot^-$, $^1\text{O}_2$, and h^+ are the major oxidizing species in the 5 wt% PI-g-C₃N₄/PMS/Vis system for BPA degradation.

To further investigate the reactive species, a series of ESR experiments were performed. Spin-trapping reagents (DMPO, BMPO, and TEMP) were employed to measure the production of reactive species during the photocatalysis process. As shown in Fig. 11a, with the addition of 5 mM PMS, both $\cdot\text{OH}$ and SO_4^{2-} signals are observed in the 5 wt% PI-g-C₃N₄/PMS/Vis system. The results show that PMS can be activated to generate SO_4^{2-} and $\cdot\text{OH}$. The ESR signals of BMPO- $\text{O}_2\cdot^-$ detected in the 5 wt% PI-g-C₃N₄/PMS/Vis system are much stronger than the signals for SO_4^{2-} and $\cdot\text{OH}$ (Fig. 11b). When 5 mM TEMP is used as the spin trapping agent, strong ESR signals for $^1\text{O}_2$ are observed (Fig. 11c). Therefore, $\text{O}_2\cdot^-$ and $^1\text{O}_2$ are likely the main species responsible for the degradation of BPA.

It has been reported that the Z-scheme heterojunction of 5 wt% PI-g-C₃N₄ can produce charge separation with the hole populated to the lower VB and electron to the higher CB, thus enhancing the redox reaction ability of the photogenerated carriers [24]. The photogenerated h^+ can directly oxidize BPA, while the photogenerated e^- can activate PMS to generate active radicals to destruct BPA.

Based on the above results, a feasible degradation mechanism of BPA in the 5 wt% PI-g-C₃N₄/PMS/Vis system is proposed (Fig. 12). First of all, e^- and h^+ can be obtained from PI-g-C₃N₄ under visible light irradiation through Eq. (5) [59]. The removal efficiency of BPA in the presence of O_2 is remarkably higher than blank condition and in the presence of N_2 (Fig. S6). This observation implies that dissolved oxygen

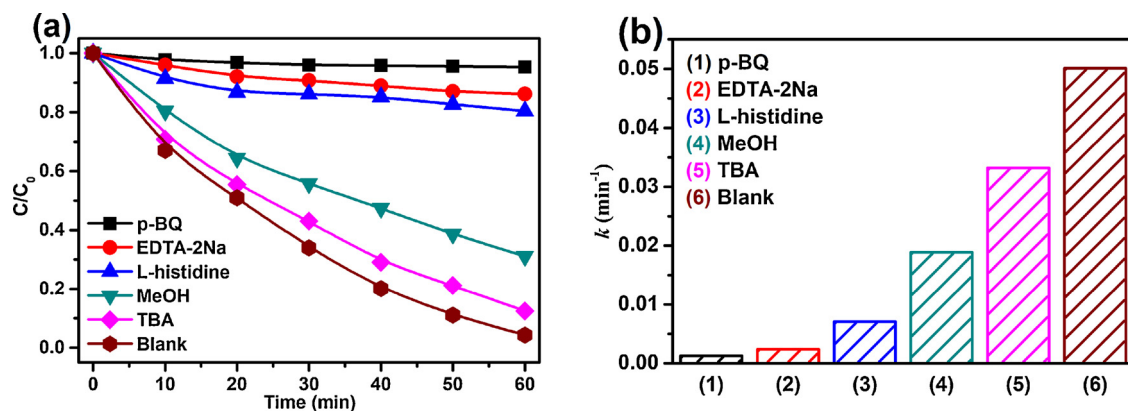
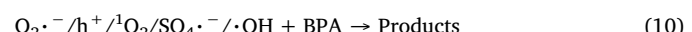
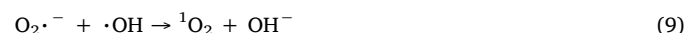


Fig. 10. (a) The degradation of BPA in the presence of different scavengers and (b) the corresponding kinetic constants in the 5 wt% PI-g-C₃N₄/PMS/Vis system. Conditions: [BPA]₀ = 10 mg/L, [PMS] = 5 mM, [Cat.] = 1 g/L, $\lambda > 400$ nm, ambient temperature, no buffer.

(O₂) in water played an important role in the degradation of BPA, due to e⁻ reacts with the adsorbed O₂ to form O₂^{·-} (Eq. (6)) [60–62]. Meanwhile, e⁻ can also be trapped by PMS to produce SO₄²⁻⁻, thus enhancing the separation efficiency of photogenerated electron-hole pairs (Eq. (7)) [63]. And more importantly, the formed SO₄²⁻⁻ can trigger the reaction between ·OH and O₂^{·-} to yield the high active ¹O₂ (Eqs. (8) and (9)) [64–66]. These reactive species contribute to the degradation of BPA molecule (Eq. (10)).



3.6. Proposed degradation pathway of BPA in the 5 wt% PI-g-C₃N₄/PMS/Vis system

To understand the BPA degradation pathway in the 5 wt% PI-g-C₃N₄/PMS/Vis system, the generated intermediates were detected by UPLC-Q-TOF-MS. Seven aromatic intermediates, 4-cumylphenol, dibenzene, 4-isopropenylphenol, prop-1-en-2-ylbenzene, hydroquinone, styrene, and phenol were detected in the reaction (the mass spectra of

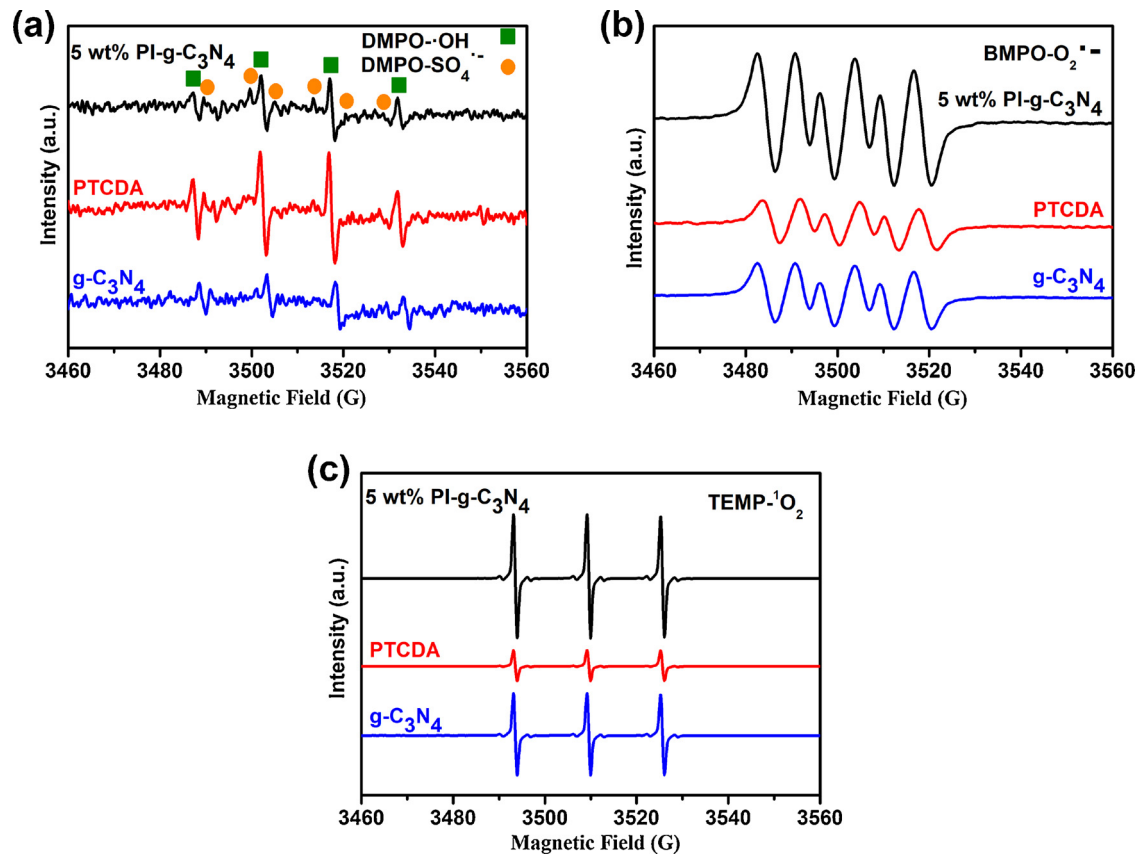
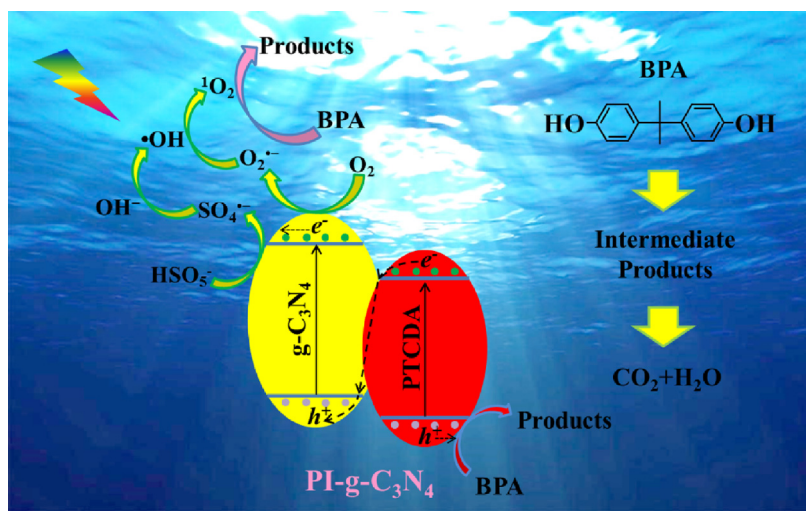
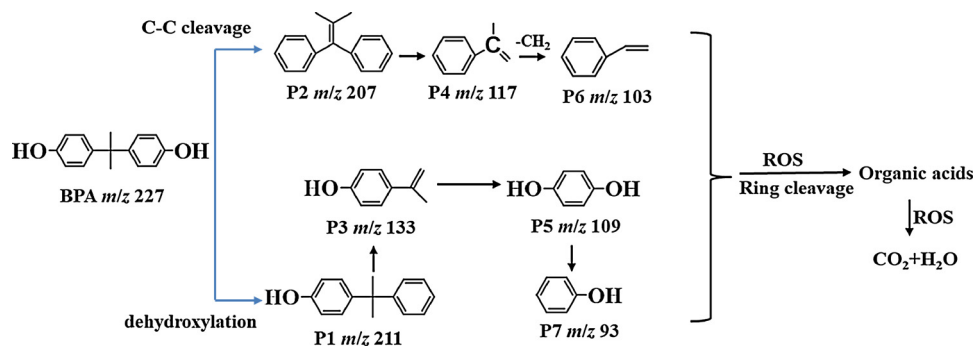
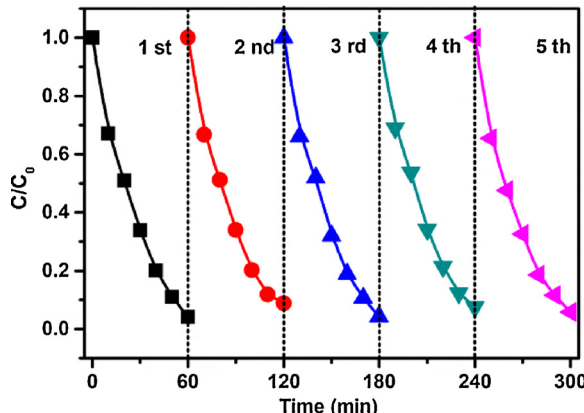


Fig. 11. ESR spectra of different photocatalysts in the presence of PMS under visible light irradiation using (a) DMPO, (b) BMPO, and (c) TEMP as the spin-trapping agent. Conditions: [Cat.] = 0.1 g/L, [PMS] = 5 mM, [DMPO] = 160 mM, [BMPO] = 25 mM, [TEMP] = 5 mM, $\lambda > 400$ nm, ambient temperature, no buffer.

Fig. 12. Possible photocatalytic mechanism in the 5 wt% PI-g-C₃N₄/PMS/Vis system.Fig. 13. Proposed BPA degradation pathways in the 5 wt% PI-g-C₃N₄/PMS/Vis system.Fig. 14. Cycling experiments for BPA degradation with 5 wt% PI-g-C₃N₄/PMS/Vis. Conditions: [BPA]₀ = 10 mg/L, [PMS] = 5 mM, [Cat.] = 1 g/L, $\lambda > 400$ nm, ambient temperature, no buffer.

all intermediates are shown in Fig. S7). The possible chemical structures and main mass fragment ions (m/z) of these reaction intermediates are shown in Table S1. According to these obtained intermediates, two possible degradation pathways for BPA are proposed (Fig. 13). The BPA degradation in the PI-g-C₃N₄/PMS/Vis system involves the breakage of C–C bonds, elimination reactions, $\cdot\text{OH}/\text{SO}_4^{\cdot-}$ group additions, dihydroxylations, etc. [67]. Two possible routes are proposed. One route would be the C–C cleavage pathway. First, the C–O bonds in BPA would be attacked by ROS, resulting in the loss of two hydroxyl groups, thus forming P2. Then, P2 would be transformed into P4 by cleavage of the C–C bond between the two benzene rings.

Later, P4 would lose the CH group to generate P6 (styrene, $m/z = 103$). Another degradation route might be a dihydroxylation pathway, where the C–O bond would be attacked by reactive active species, affording P1. Then, the reactive species would attack the electron-rich groups in P1 to generate P3. Furthermore, P3 would then be oxidized to generate P5, which would be subsequently transformed into P7 [68]. Finally, all the intermediate products could be further oxidized to small molecules such as formic, acetic, oxalic, and then mineralized into CO_2 and H_2O during the photocatalytic degradation process [69].

3.7. Stability of the 5 wt% PI-g-C₃N₄ photocatalyst

Reusability is also an important issue for catalysts. This was examined by running the same photocatalytic removal experiment continuously in multiple cycles in the presence of PMS. The catalyst was easily separated through a Millipore filter (pore size of 0.22 μm) after the reaction, and then washed with Milli-Q water several times, dried in a vacuum oven, and finally kept at ambient temperature. Repeated experiments were run by adding a fresh solution of BPA and PMS. As shown in Fig. 14, the degradation efficiency of BPA remains almost unchanged after five successive cycles, indicating the high stability of 5 wt% PI-g-C₃N₄.

4. Conclusions

In this study, a metal-free photocatalyst (PI-g-C₃N₄) was prepared via an amidation reaction, which exhibited higher photocatalytic activities than the individual PTCDA and g-C₃N₄. With the addition of PMS, the photocatalytic degradation efficiency of BPA by 5 wt% PI-g-C₃N₄ was greatly enhanced; the pseudo-first-order degradation kinetics

constant of BPA was increased from 0.0057 to 0.0501 min⁻¹. The improved activity can be attributed to a more effective separation efficiency of photogenerated electron-hole pairs and the higher conductivity of 5 wt% PI-g-C₃N₄, which promoted the activation of PMS into active radicals via the photogenerated electrons. Rather than SO₄²⁻ radicals, O₂^{•-}, ¹O₂, and h⁺ were mainly responsible for the degradation of BPA in the 5 wt% PI-g-C₃N₄/PMS/Vis system. The high stability of the 5 wt% PI-g-C₃N₄ was also exhibited.

Acknowledgement

This work was supported by the National Natural Science Foundation of China (Project No. 21777176, 51578532).

Appendix A. Supplementary data

Supplementary material related to this article can be found, in the online version, at doi:<https://doi.org/10.1016/j.apcatb.2018.06.049>.

References

- [1] A. Rastogi, S.R. Al-Abed, D.D. Dionysiou, *Appl. Catal. B: Environ.* 85 (2009) 171–179.
- [2] S. Zhang, Q. Fan, H. Gao, Y. Huang, X. Liu, J. Li, X. Xu, X. Wang, *J. Mater. Chem. A* 4 (2016) 1414–1422.
- [3] Tk. Lau, W. Chu, N.J.D. Graham, *Environ. Sci. Technol.* 41 (2007) 613–619.
- [4] R.H. Waldemer, P.G. Tratnyek, R.L. Johnson, J. Nurmi, *Environ. Sci. Technol.* 41 (2007) 1010–1015.
- [5] P. Shi, R. Su, F. Wan, M. Zhu, D. Li, S. Xu, *Appl. Catal. B: Environ.* 123–124 (2012) 265–272.
- [6] J. Zou, J. Ma, L. Chen, X. Li, Y. Guan, P. Xie, C. Pan, *Environ. Sci. Technol.* 47 (2013) 11685–11691.
- [7] C. Cai, L. Wang, H. Gao, L. Hou, H. Zhang, *J. Environ. Sci.* 26 (2014) 1267–1273.
- [8] M. Mahdi-Ahmed, S. Chiron, J. Hazard. Mater. 265 (2014) 41–46.
- [9] X. Duan, K. O'Donnell, H. Sun, Y. Wang, S. Wang, *Small* 11 (2015) 3036–3044.
- [10] H. Sun, S. Liu, G. Zhou, H.M. Ang, M.O. Tade, S. Wang, *ACS Appl. Mater. Interfaces* 4 (2012) 5466–5471.
- [11] J. Zhang, X. Shao, C. Shi, S. Yang, *Chem. Eng. J.* 232 (2013) 259–265.
- [12] T. Xiong, W. Cen, Y. Zhang, F. Dong, *ACS Catal.* 6 (2016) 2462–2472.
- [13] S. Fang, Y. Xia, K. Lv, Q. Li, X. Li, J. Sun, M. Li, *Appl. Catal. B: Environ.* 185 (2016) 225–232.
- [14] Y. Tao, Q. Ni, M. Wei, D. Xia, X. Li, A. Xu, *RSC Adv.* 5 (2015) 44128–44136.
- [15] X. Jiang, J. Li, J. Fang, L. Gao, W. Cai, X. Li, A. Xu, X. Ruan, *J. Photochem. Photobiol. A* 336 (2017) 54–62.
- [16] J. Cheng, Z. Hu, K. Lv, X. Wu, Q. Li, Y. Li, X. Li, J. Sun, *Appl. Catal. B: Environ.* 232 (2018) 330–339.
- [17] Y. Li, K. Lv, W. Ho, F. Dong, X. Wu, Y. Xia, *Appl. Catal. B: Environ.* 202 (2018) 611–619.
- [18] K.Y.A. Lin, Z.Y. Zhang, *Chem. Eng. J.* 313 (2017) 1320–1327.
- [19] Y. Wang, X. Zhao, D. Cao, Y. Wang, Y. Zhu, *Appl. Catal. B: Environ.* 211 (2017) 79–88.
- [20] B. Liu, M. Qiao, Y. Wang, L. Wang, Y. Gong, T. Guo, X. Zhao, *Chemosphere* 189 (2017) 115–122.
- [21] M.J. Robb, B. Newton, B.P. Fors, C.J. Hawker, *J. Org. Chem.* 79 (2014) 6360–6365.
- [22] K. Nagarajan, A.R. Mallia, K. Muraleedharan, M. Hariharan, *Chem. Sci.* 8 (2017) 1776–1782.
- [23] Y. Avlasevich, C. Li, K. Müllen, *J. Mater. Chem.* 20 (2010) 3814.
- [24] G. Dong, L. Yang, F. Wang, L. Zang, C. Wang, *ACS Catal.* 6 (2016) 6511–6519.
- [25] G. Dong, L. Zhang, *J. Phys. Chem. C* 117 (2013) 4062–4068.
- [26] J. Xu, Y. Wang, Y. Zhu, *Langmuir* 29 (2013) 10566–10572.
- [27] D. Tang, G. Zhang, *Appl. Surf. Sci.* 391 (2017) 415–422.
- [28] Y. Zheng, L. Lin, X. Ye, F. Guo, X. Wang, *Angew. Chem. Int. Ed.* 53 (2014) 11926–11930.
- [29] K. Wang, G. Zhang, J. Li, Y. Li, X. Wu, *ACS Appl. Mater. Interfaces* 9 (2017) 43704–43715.
- [30] Y. Li, K. Lv, W. Ho, Z. Zhao, Y. Huang, *Chin. J. Catal.* 38 (2017) 321–329.
- [31] X. Bai, L. Wang, Y. Wang, W. Yao, Y. Zhu, *Appl. Catal. B: Environ.* 152–153 (2014) 262–270.
- [32] S.J. Park, K. Li, F.L. Jin, *Mater. Chem. Phys.* 108 (2008) 214–219.
- [33] J. Li, B. Shen, Z. Hong, B. Lin, B. Gao, Y. Chen, *Chem. Commun.* 48 (2012) 12017–12019.
- [34] Y. Li, W. Ho, K. Lv, B. Zhu, S.C. Lee, *Appl. Surf. Sci.* 430 (2018) 380–389.
- [35] S. Rangan, C. Ruggieri, R. Bartynski, J.I. Martinez, F. Flores, J. Ortega, *J. Phys. Chem. B* 122 (2018) 534–542.
- [36] S. Dong, L. Xia, T. Guo, F. Zhang, L. Cui, X. Su, D. Wang, W. Guo, J. Sun, *Appl. Surf. Sci.* 445 (2018) 30–38.
- [37] F. Wu, H. Huang, T. Xu, W. Lu, N. Li, W. Chen, *Appl. Catal. B: Environ.* 218 (2017) 230–239.
- [38] Z. Lin, G. Waller, Y. Liu, M. Liu, C.-P. Wong, *Adv. Energy Mater.* 2 (2012) 884–888.
- [39] Z. Ding, X. Chen, M. Antonietti, X. Wang, *ChemSusChem* 4 (2011) 274–281.
- [40] Z. Huang, Q. Sun, K. Lv, Z. Zhang, M. Li, B. Li, *Appl. Catal. B: Environ.* 164 (2015) 420–427.
- [41] Z. Qin, J. Zhang, H. Zhou, Y. Song, T. He, *Nucl. Instrum. Methods B* 170 (2000) 406–412.
- [42] H. Shao, X. Zhao, Y. Wang, R. Mao, Y. Wang, M. Qiao, S. Zhao, Y. Zhu, *Appl. Catal. B: Environ.* 218 (2017) 810–818.
- [43] G. Wang, S. Chen, X. Quan, H. Yu, Y. Zhang, *Carbon* 115 (2017) 730–739.
- [44] P. Hu, M. Long, *Appl. Catal. B: Environ.* 181 (2016) 103–117.
- [45] Y. Wang, D. Cao, X. Zhao, *Chem. Eng. J.* 328 (2017) 1112–1121.
- [46] M. Sayed, J.A. Khan, L.A. Shah, N.S. Shah, F. Shah, H.M. Khan, P. Zhang, H. Arandian, *J. Phys. Chem. C* 122 (2018) 406–421.
- [47] H.V. Lutze, N. Kerlin, T.C. Schmidt, *Water Res.* 72 (2015) 349–360.
- [48] C. Feng, Z. Wang, Y. Ma, Y. Zhang, L. Wang, Y. Bi, *Appl. Catal. B: Environ.* 205 (2017) 19–23.
- [49] S. Kumar, A. Baruah, S. Tonda, B. Kumar, A. Baruah, V. Shanker, *J. Phys. Chem. C* 117 (2013) 26135–26143.
- [50] X. Hao, Z. Jin, H. Yang, G. Lu, Y. Bi, *Appl. Catal. B: Environ.* 210 (2017) 45–56.
- [51] L. Yang, G. Dong, D.L. Jacobs, Y. Wang, L. Zang, C. Wang, *J. Catal.* 352 (2017) 274–281.
- [52] A. Mitra, P. Howli, D. Sen, B. Das, K.K. Chattopadhyay, *Nanoscale* 8 (2016) 19099–19109.
- [53] J. Lu, Y. Wang, F. Liu, L. Zhang, S. Chai, *Appl. Surf. Sci.* 393 (2017) 180–190.
- [54] G.P. Anipstakis, D.D. Dionysiou, *Environ. Sci. Technol.* 37 (2003) 4790–4797.
- [55] G. Liu, S. You, Y. Tan, N. Ren, *Environ. Sci. Technol.* 51 (2017) 2339–2346.
- [56] S. Fang, K. Lv, Q. Li, H. Ye, D. Du, M. Li, *Appl. Surf. Sci.* 358 (2015) 336–342.
- [57] T. Zhang, W. Lei, P. Liu, J.A. Rodriguez, J. Yu, Y. Qi, G. Liu, M. Liu, *J. Phys. Chem. C* 120 (2016) 2777–2786.
- [58] S. Dong, Y. Cui, Y. Wang, Y. Li, L. Hu, J. Sun, J. Sun, *Chem. Eng. J.* 294 (2014) 102–110.
- [59] S.C. Yan, Z.S. Li, Z.G. Zou, *Langmuir* 26 (2010) 3894–3901.
- [60] J. Li, J. Fang, P. Ye, D. Wu, M. Wang, X. Li, A. Xu, *J. Photochem. Photobiol. A* 342 (2017) 85–93.
- [61] S. Dong, X. Ding, T. Guo, X. Yue, X. Han, J. Sun, *Chem. Eng. J.* 316 (2017) 778–789.
- [62] C. Yu, K. Wang, P. Yang, S. Yang, C. Lu, Y. Song, S. Dong, J. Sun, J. Sun, *Appl. Surf. Sci.* 420 (2017) 233–242.
- [63] N. Jaafarzadeh, F. Ghanbari, M. Ahmadi, *Chem. Eng. J.* 320 (2017) 436–447.
- [64] C. Qi, X. Liu, C. Lin, H. Zhang, X. Li, J. Ma, *Chem. Eng. J.* 315 (2017) 201–209.
- [65] L. Zhou, W. Song, Z. Chen, G. Yin, *Environ. Sci. Technol.* 47 (2013) 3833–3839.
- [66] D. Tang, G. Zhang, S. Guo, *J. Colloid Interface Sci.* 454 (2015) 44–51.
- [67] C. Li, X.Z. Li, N. Graham, N.Y. Gao, *Water Res.* 42 (2008) 109–120.
- [68] Q. Han, H. Wang, W. Dong, T. Liu, Y. Yin, H. Fan, *Chem. Eng. J.* 262 (2015) 34–40.
- [69] Y. Wang, J. Li, J. Sun, Y. Wang, X. Zhao, *J. Mater. Chem. A* 5 (2017) 19151–19158.